Electrodeposition of luminescent composite metal coatings containing rare-earth phosphor particles

Murugan Ganapathi [a], *Svetlana V. Eliseeva* [b], *Neil R. Brooks* [b], *Dimitri Soccol* [b], *Jan Fransaer* [b], *Koen Binnemans* [b]

[a] Katholieke Universiteit Leuven, Department of Metallurgy and Materials Engineering (MTM), Kasteelpark Arenberg 44 - P.O. Box 2450, B-3001 Heverlee (Belgium)

[b] Katholieke Universiteit Leuven, Department of Chemistry, Celestijnenlaan 200F - P.O. Box 2404, B-3001 Heverlee (Belgium

Abstract

Mixtures of acetamide and dimethylsulfone ($DMSO_2$) with dissolved anhydrous transition metal chlorides are introduced as new non-aqueous electrolytes for the preparation of composite metal coatings with embedded hydrophilic particles via an electrolytic co-deposition process. Red-emitting (Eu_2O_3 and $Y_2O_3:Eu^{3+}$), yellow-emitting ($Y_3Al_5O_{12}:Ce^{3+}$), green-emitting ($Gd_2O_2S:Tb^{3+}$) and blue-emitting ($BaMg_2Al_{16}O_{27}:Eu^{2+}$) rare-earth phosphor particles and yttrium oxide particles have been embedded into thin nickel and cobalt layers. The metal coatings with the rare-earth phosphor particles have a metallic lustre, but show at the same time photoluminescence upon irradiation with UV light. The spectroscopic and photophysical properties of the rare-earth phosphors are not modified by embedding them in the metallic host matrix. Different electrodeposition parameters were optimised in order to obtain well-adherent coatings with a uniform particle distribution. By preparing mixtures of the $Y_2O_3:Eu^{3+}$ and $Gd_2O_2S:Tb^{3+}$ phosphors, the emission colour could be varied from red over orange and yellow to green, depending on the mixing ratios. Embedding mixtures of yellow and blue phosphors in the metal layer made it possible to produce coatings with white photoemission.

Keywords: co-deposition; composite materials; electrodeposition; electroplating; lanthanides; luminescence; non-aqueous electrolytes; rare earths.

Introduction

Composite metal coatings consist of small particles incorporated into a metallic matrix[1]. Such coatings can be prepared via an electrolytic or an electroless deposition process, and the small particles (of micrometer or nanometer size) are intentionally added to the plating bath. The main purposes of the co-deposited particles are to improve the corrosion or wear resistance of metallic layers, or to improve the mechanical properties of these coatings. For instance, nickel coatings with silicon carbide or diamond particles have a superior abrasion resistance.[2] Such coatings are applied as cylinder linings in aluminium automobile engines to improve the wear resistance. NiCo-Cr_2O_3 coatings enhance the corrosion resistance of turbine blades in aero gas-turbine engines. Co-deposition of polytetrafluoroethylene (PTFE) with nickel, nickel alloys or copper results in coatings with very low friction coefficients[3]. The co-deposition of particles in metal layers not only modifies the mechanical or physicochemical properties of the layers, but the particles can also add other functionalities to the coatings. Light-emitting composite coatings can be obtained by adding luminescent particles to the plating bath. Luminescent nickel coatings were first prepared by Feldstein via an electroless deposition process.[4] Coatings with calcium tungstate phosphor particles showed a blue emission upon UV irradiation (254 nm), while coatings with calcium halophosphate phosphor particles emitted a whitish light.[5] Das *et al.* made red-emitting nickel coatings containing $YVO_4:Eu^{3+}$ phosphor particles via an electroless process from an aqueous plating bath.[6] The maximum loading of phosphor particles was 14.5% (v/v). Advantages of selecting rare-earth-containing particles as luminophors are the high colour purity due to the line emission by the trivalent rare-earth (lanthanide) ions and the possibility to tune the emission colour by an appropriate choice of the rare-earth ion.[7] Although luminescent composite coatings have received only little attention so far, these advanced materials can have several interesting applications.[8] For wear indication, they can be applied as a coating between the substrate and a functional top coating. If inspection with a handheld UV-lamp shows the luminescence of the undercoating, it means that the functional coating is worn out and that recoating is needed. Alternatively, the luminescent particles can be incorporated into the functional top layer itself. In that case, the disappearance of the luminescence is a sign of wear. Luminescent composite coatings can also be used as authentication marker for discrimination between genuine and counterfeit components or objects. Finally, luminescent coatings are esthetically appealing. It should be mentioned that incorporation of rare-earth oxide particles improves the microstructure, hardness and wear resistance of nickel nanocomposite coatings.[9]

Electrodeposition is often a superior process compared to electroless deposition for the preparation of composite coatings, because the former is much faster and allows better control of the deposition process. However, rare-earth phosphor particles are hydrophilic and it is difficult to incorporate hydrophilic particles (e.g. silica) in metal coatings from an aqueous electroplating bath, due to the presence of a hydration layer on their surface.[10] This hydration layer prevents the particles making direct contact with the electrode. Small gaps remain between these particles and the electrode. Metal ions diffuse into these gaps and are reduced on the electrode underneath the particle. Instead of being incorporated into the metal coating, the particles are pushed up by the moving metal/electrolyte boundary. In addition, small particles can aggregate in an aqueous solution. One of us has shown that hydrophilic particles can be co-deposited from non-aqueous electrolytes.[11] For instance, aluminium coatings containing hydrophilic SiO_2 nanoparticles were obtained via an electrolytic process from an $AlCl_3/DMSO_2$ ($DMSO_2$ = dimethylsulfone) electrolyte.

In this paper, we describe how luminescent nickel and cobalt coatings containing red-, yellow-, green- or blue-emitting rare-earth phosphor particles can be prepared by co-deposition from a new non-aqueous electrolyte consisting of mixtures of acetamide and dimethylsulfone, to which anhydrous metal chlorides

have been added. Different deposition parameters were optimised to get well adherent coatings with a uniform particle distribution. The morphology of the coatings was characterised by scanning electron microscopy (SEM) and the emission properties were investigated by steady-state and time-resolved luminescence spectroscopy. The binary phase diagram of acetamide-$DMSO_2$ has been determined.

Experimental Section

Preparation of electrolyte

Dimethylsulfone ($DMSO_2$, 99%, Alfa Aesar), acetamide (99%, Alfa Aesar) and anhydrous $NiCl_2$ and $CoCl_2$ were used for the preparation of the electrolyte. Anhydrous $NiCl_2$ and $CoCl_2$ were prepared by dehydrating the hydrated salts in an oven at 260 °C. Dimethylsulfone and acetamide were dried before use at 110 °C for 12 hours in a hot air oven, followed by vacuum drying at room temperature for 12 hours. To avoid extensive evaporation of acetamide during the drying procedure in the oven, the container with acetamide was covered with a lid and opened from time to time. Y_2O_3 and Eu_2O_3 (99.99%) were from Rare Earth Products Ltd. The rare-earth phosphors Y_2O_3:Eu^{3+} (red phosphor), $Y_3Al_5O_{12}$:Ce^{3+} (yellow phosphor), Gd_2O_2S:Tb^{3+} (green phosphor), and $BaMg_2Al_{16}O_{27}$:Eu^{2+} (blue phosphor) were obtained from Phosphor Technology Ltd (Stevenage, Hertfordshire, UK). Y_2O_3 and rare-earth phosphor particles were dried at 200 °C for 12 hours and dispersed in the electrolyte mixture. Mixtures of phosphors were prepared by thorough grinding in an agate mortar of the corresponding phosphors in an appropriate weight ratio. The melt was prepared in an argon circulated glove box. The composition of the molten electrolytes was acetamide:$DMSO_2$:$NiCl_2$ (0.593: 0.391:0.016 molar fractions) for the nickel plating bath and acetamide:$DMSO_2$:$CoCl_2$ (0.617:0.366:0.017 molar fractions) for the cobalt plating bath. The acetamide:$DMSO_2$ ratio is not critical, although all electrolytes had an excess of acetamide relative to $DMSO_2$. It should be noted that the deposition temperature of 130 °C is above the melting point of both acetamide and $DMSO_2$, so there would be no benefit of using a low-melting eutectic mixture (with 0.80 mole fraction of acetamide).

Electrodeposition experiments

Nickel or cobalt rods (Chempur, 5 mm, 99.99%) were used as counter and reference electrodes. Rectangular pieces of a silicon wafer covered with a copper top layer were used as the working electrode, on which the composite metal coatings were deposited. The three-neck electrolyte cell which was used had a total volume of 40 mL and an electrolyte volume of 15 mL. Prior to deposition experiments all electrodes were cleaned by the following procedure: (1) degreasing by soaking them in a solution of an alkaline cleaner (P3-RST Henkel) at 70 °C for 5 minutes; (2) rinsing with deionised water; (3) immersing in a HNO_3 solution (10 vol.%) to remove the residual oxide layer on the surface of the electrodes; (4) rinsing with deionised water; (5) washing with absolute ethanol and acetone; (6) drying in a stream of warm air. After the drying step, the electrodes were transferred into a glove box. All electrochemical experiments were performed using a Potentiostat/Galvanostat EG&G 273 and a Solartron Instruments SI 1287 electrochemical interface. Typical experiments were performed at a temperature of 130 °C, with a particle loading of 80 g L^{-1}. These parameters were set after optimisation experiments at varying temperatures and particle loading of the electrolyte bath. The molten electrolyte was stirred with a magnetic stirrer (250 rpm) to keep the particles in suspension during the electrodeposition process. The electrodeposition experiments

were carried out potentiostatically rather than galvanostatically, because this allows a more precise control of the electrochemical reaction during the electrolysis. The electrodeposition was performed at a potential of -0.4 V versus Ni for nickel deposition and -0.4 V versus Co for cobalt deposition, after optimisation experiments had shown that these potential values gave coatings of a good quality. After the electrodeposition experiments, the samples were taken from the electrolyte solution, removed from the glove box, and immediately washed with copious amounts of deionised water and ethanol, and finally dried in a hot air oven at 110 °C, followed by one day in a vacuum desiccator. The surface area of the nickel deposits on the copper substrate was 10 mm by 10 mm. The electrodeposition experiments were stopped after a charge of 20 C cm^{-2} had passed through the working electrode, which corresponds to a theoretical thickness *t* of 6.8 μm, assuming a current efficiency of 100%. This thickness has been selected to make sure that the thickness of the metal coating is larger than the average size of the phosphor particles (1 to 3 μm).

Characterisation techniques

Thermal analysis experiments were performed on a TA Instruments SDT Q600 (Simultaneous DSC and TGA) or on a Mettler-Toledo DSC822 module. The morphology and elemental composition of the composite metal deposits were determined by scanning electron microscopy (SEM) and energy-dispersive X-ray analysis (EDX) on a Philips XL 30 FEG apparatus. The doping concentration of europium and terbium in the phosphor particles has been measured by Inductively Coupled Plasma Optical Emission Spectroscopy (ICP-OES) on a Varian 720 ES apparatus. The excitation and luminescence spectra were recorded at room temperature on an Edinburgh Instruments FLS920 spectrofluorimeter, with a xenon arc lamp (450 W) as excitation source, a double excitation monochromator, and a Hamamatsu R2658P photomultiplier. All spectra are corrected for the instrumental functions. For luminescence decay measurements, the sample was excited by a μF900H microsecond xenon flash lamp, having an optical pulse width between 1.5 and 2.5 μs, and an average power of 60 W. An excitation wavelength of the xenon flash lamp can be selected by the excitation monochromator, and was set at 254 nm. For Eu^{3+}-containing samples emission has been monitored at 611 nm ($^5D_0 \rightarrow {}^7F_2$ transition), while for Tb^{3+} at 545 nm ($^5D_4 \rightarrow {}^7F_5$ transition). The luminescence decay curves were analysed with the F900 software program of Edinburgh Instruments. It is discussed further on in the text that the general appearance of the excitation spectra, and mainly the relative intensity of the charge transfer or host-centred transitions compared to the f-f transitions, depends on the thickness of the powder layer, but the emission spectra remain the same. However, to be consequent, the phosphor powders were placed between two quartz plates with an average thickness of the layer of about 200 μm and then inserted into the home-made sample holder for measurements.

Results and Discussion

The electrolytes used for the deposition of the composite coatings were based on binary mixtures of $DMSO_2$ and acetamide, with dissolved anhydrous metal chlorides. Electrical conduction is achieved by (partial) dissociation of the dissolved metal salts. Although several research reports describe the use of $DMSO_2$ in combination with metal chlorides as non-aqueous solvents for electrolyte bath for the deposition, electrolytes based on mixtures of $DMSO_2$ and acetamide have not been described in the literature.[12] Previously, acetamide-urea-NaBr-KBr melts have been applied for the deposition of alloys of rare earths.[13] The performance of the acetamide- $DMSO_2$ electrolyte for electrodeposition of the composite coatings is better than that of $DMSO_2$ and acetamide separately. The presence of $DMSO_2$ strongly reduces the evaporation of acetamide at temperatures above 90 °C, although the use of closed electrodeposition cells is recommended to further reduce the evaporation of acetamide. The melting point of a mixture of $DMSO_2$ and acetamide depends on the mole fraction of each component. The binary phase diagram of $DMSO_2$-acetamide (Figure 1) was constructed by differential scanning calorimetry (DSC) and was found to exhibit classic eutectic behaviour. The eutectic composition has been determined by applying *Tammann's method*.[14] In this method, the enthalpy of the eutectic melting peak is plotted as a function of the composition (*Tammann plot*, Figure 2).[15]The *x*-coordinate of the crossing point of the two extrapolated straight lines fitted through the data points gives the eutectic composition. The eutectic composition was found to lie at 0.80 mole fraction of acetamide. The eutectic temperature was found to be 52.5 °C, which is considerably lower than the melting points of pure $DMSO_2$ (110 °C) and acetamide (79-81 °C). The solvent mixture can be used for electrodeposition between 65 and 140 °C. Above 140 °C, excessive evaporation of the solvent components, and especially of acetamide, is observed. The electric conductivity of an electrolyte with acetamide:$DMSO_2$:$NiCl_2$ in the mole fractions 0.593: 0.391:0.016 was determined as a function of temperature by AC impedance measurements. The conductivity of the melt (melting point: 63 °C) increases as a function of temperature, due to a decrease in viscosity and a consequent increase in the mobility of the ions (Figure 3). The conductivity is about a factor of 10 lower than the conductivity of aqueous nickel plating electrolytes.

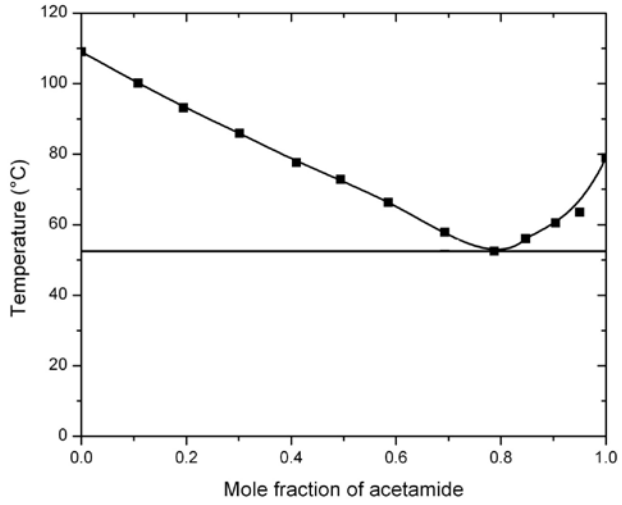

Figure 1. Phase diagram of the acetamide-$DMSO_2$ binary system.

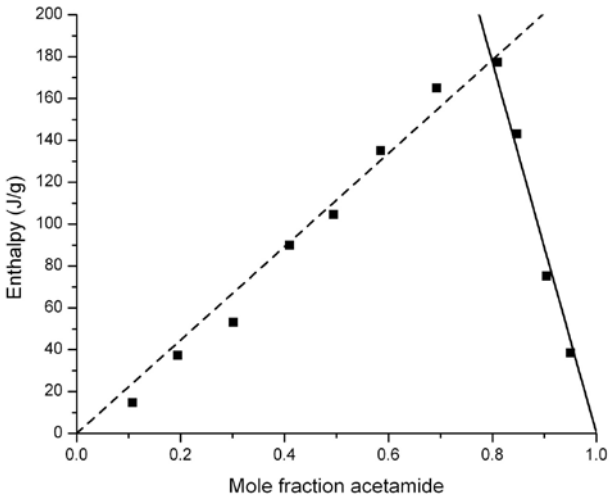

Figure 2. Tammann plot for the acetamide-$DMSO_2$ binary system.

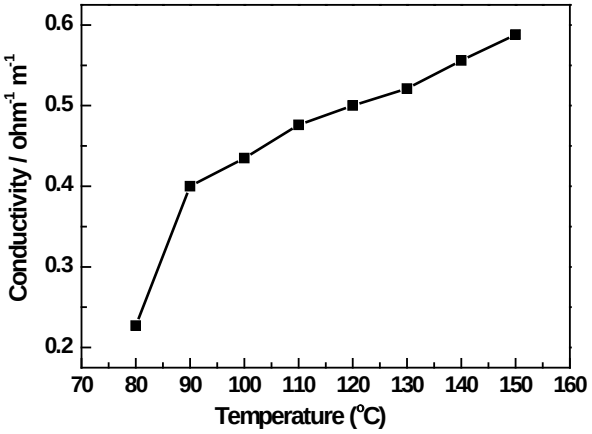

Figure 3. Electric conductivity of the acetamide-$DMSO_2$-$NiCl_2$ electrolyte (0.593: 0.391:0.016 mole fraction of acetamide:$DMSO_2$:$NiCl_2$) as a function of temperature.

The composite nickel coatings were deposited on a copper working electrode, and the reference and counter electrode were both made of nickel. During the electrodeposition process, the particles were kept dispersed in the electrolyte by stirring the plating bath with a magnetic stirrer. The electrodeposition process was performed at a constant potential versus a nickel reference electrode. It was found that it is possible to deposit Ni and Ni-Y_2O_3 coatings outside of the glove box under the same experimental conditions as those used for electrodeposition inside the glove box, but SEM analysis of the coatings showed that the quality of the coatings obtained outside the glove box were of an inferior quality (less compact coatings and poorer embedding of particles in the metallic matrix). Therefore, the depositions were routinely performed in an argon-filled glove box. The influence of different parameters on the composition and quality of the composite nickel coatings was investigated for Ni-Y_2O_3 coatings in order to optimise the deposition process. The concentration of Y_2O_3 particles dispersed in the electrolyte was varied between 13 g L^{-1} and 100 g L^{-1}. Experiments performed at a deposition potential of –0.4 V versus a nickel electrode show an increase of particle loading in the nickel coatings as the particle content is raised from 2 to 45 vol.% Y_2O_3 (Table 1). For most experiments, a particle concentration of 80 g L^{-1} was used, which results in a concentration of about 40 vol. % of phosphor particles (42 vol.% for Y_2O_3) in the coating.

Variation of the deposition potential revealed that at potentials more negative than –0.4 V versus Ni, the amount of incorporated Y_2O_3 particles stayed constant, while it decreased as a function of the deposition potential for potentials less negative than –0.4 V versus Ni. No pure nickel or Ni-Y_2O_3 deposits could be obtained at 0 V versus Ni. On the basis of these experiments, a deposition potential of –0.4 V versus Ni was chosen for further experiments. An increase of the temperature from 130 °C to 150 °C decreased the content of Y_2O_3 in the nickel coatings from 45 to 35 vol.% for an electrolyte bath with an Y_2O_3 concentration of 100 g L^{-1}. Moreover, the coatings deposited at temperatures of 140 °C and higher showed a poorer adherence than those obtained at 130 °C. In order to improve mass transport, the deposition was performed at the highest temperature that still allows obtaining good quality deposits, so that 130 °C was found to be the optimum temperature for deposition. The microstructure of the nickel coatings was investigated by scanning electron microscopy (SEM) and the elemental composition of the phases was analysed by energy-dispersive X-ray spectroscopy (EDX). In Figure 4, a representative example of a SEM image of a nickel coating with Y_2O_3 particles is shown. The nickel matrices are smooth and without cracks. The irregularly shaped Y_2O_3 particles are embedded in this matrix. The Ni-Eu_2O_3 samples looked quite different from the Ni-Y_2O_3 samples in the sense that more Eu_2O_3 particles were covered by a nickel layer than the Y_2O_3 particles. This may be due to the electrically conductive behaviour of the Eu_2O_3 particles.

Table 1. Effect of particle concentration in the electrolyte bath on the vol.% of Y_2O_3 particles in Ni-Y_2O_3 coatings.[(a)]

concentration of Y_2O_3 (g L^{-1})	atomic % of O	atomic % of Y	atomic % of Ni	vol.% of Y_2O_3
13	5.8	0.5	93.7	2
26	7.2	1.7	91.1	6
39	9.8	4.6	85.6	15
52	14.3	10.1	75.6	31
65	15.4	13.2	71.4	39
80	17.5	14.2	68.3	42
100	19.4	15.4	65.2	45

(a) Deposition conditions: (1) potential : –0.4 V vs. Ni; (2) stirring speed: 250 rpm; (3) temperature: 130 °C; (4) substrate: copper electrode; (5) electrolyte: acetamide:$DMSO_2$: $NiCl_2$ (0.593: 0.391:0.016 molar fractions).

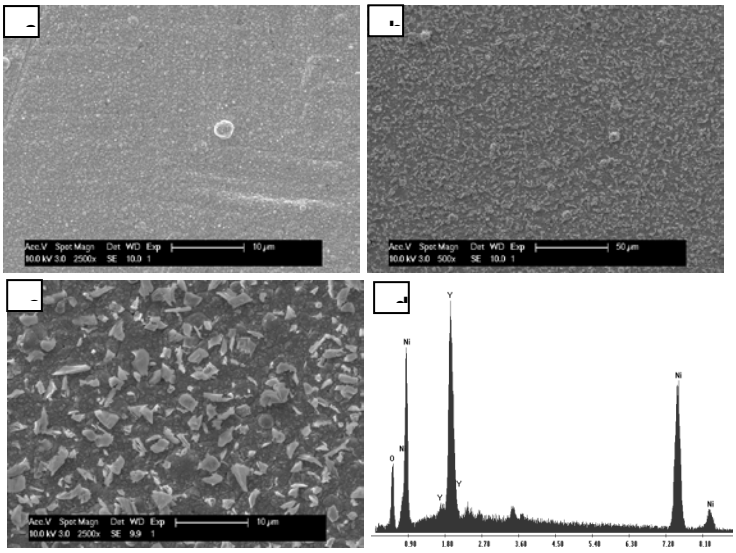

Figure 4. Ni and Ni-Y_2O_3 coatings deposited at potential of –0.4 V vs. Ni with stirring at 130 °C. An amount of 80 g L^{-1} of Y_2O_3 was added to the acetamide-$DMSO_2$-$NiCl_2$ electrolyte. (a) SEM image of pure Ni; (b) SEM image of Ni-Y_2O_3 at low magnification; (c) SEM image of Ni-Y_2O_3 at high magnification; (d) EDX of Ni-Y_2O_3.

In order to show that the rare-earth oxide particles can be incorporated in a metallic matrix other than nickel, the experiments of the deposition of Ni-Y_2O_3 coatings were repeated for cobalt. Cobalt coatings were deposited from an acetamide:$DMSO_2$:$CoCl_2$ electrolyte, with the mole fractions of the components in the ratios 0.617:0.366:0.017. The experimental setup was the same as for the deposition of nickel, except that cobalt was used as reference and counter electrode. Pure cobalt deposits were prepared at deposition potentials between -0.2 V and -1.4 V versus Co, although a deposition potential of –0.4 V was selected for the preparation of most of the Co-Y_2O_3 coatings. The results for the incorporation of Y_2O_3 in cobalt are very comparable to those of nickel. Visual comparison of the coatings did not reveal major differences, but SEM analysis showed that the Co-Y_2O_3 deposits are less compact than the Ni-Y_2O_3 ones.

For luminescence studies, nickel coatings with Eu_2O_3, Y_2O_3:Eu^{3+}, Gd_2O_2S:Tb^{3+}, $Y_3Al_5O_{12}$:Ce^{3+} and $BaMg_2Al_{16}O_{27}$:Eu^{2+} particles were prepared. With the exception of Eu_2O_3, these materials are widely used as rare-earth phosphors.[16] SEM pictures of the nickel coatings with the different phosphor particles show that the phosphor particles are well embedded into the metallic host matrix (Figure 5). Upon irradiation with a short-wavelength UV-lamp (254 nm), the coatings with Eu_2O_3 showed a faint red, barely visible photoluminescence, the nickel coatings with Y_2O_3:Eu^{3+} particles gave a very bright red luminescence upon irradiation at 254 nm (Figure 6). The Gd_2O_2S:Tb^{3+} and $BaMg_2Al_{16}O_{27}$:Eu^{2+} containing coatings gave a green and blue photoluminescence upon UV-irradiation, respectively (Figure 6). On the other hand, the greenish yellow photoluminescence of the coatings with the $Y_3Al_5O_{12}$:Ce^{3+} particles was very faint upon irradiation with a standard mercury lamp and became clearly visible to the naked eye only under 340 nm excitation with a xenon lamp (Figure S13, ESI).

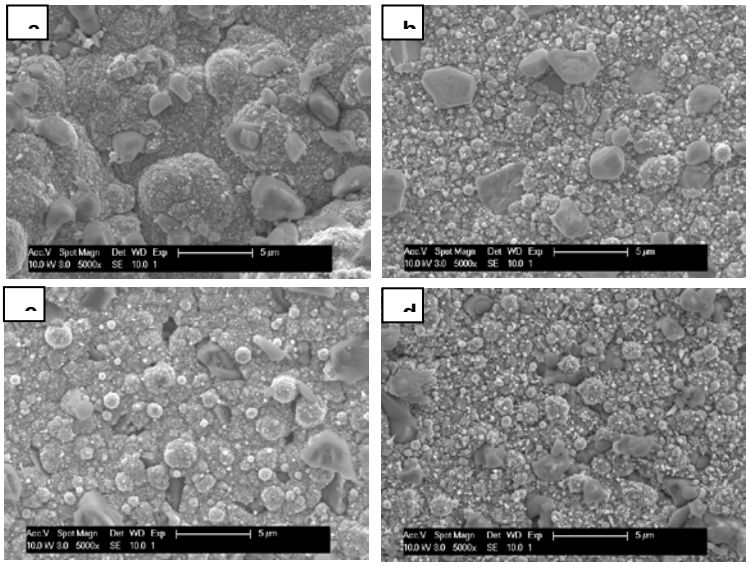

Figure 5. SEM pictures of luminescent composite nickel coatings deposited at –0.4 V vs. Ni at a temperature of 130 °C. The electrolyte was stirred at 250 rpm. (a) Nickel coating with Y_2O_3:Eu^{3+} phosphor particles ; (b) nickel coating with Gd_2O_2S:Tb^{3+} phosphor particles ; (c) nickel coating with $BaMg_2Al_{16}O_{27}$:Eu^{2+} phosphor particles; (d) nickel coating with $Y_3Al_5O_{12}$:Ce^{3+} phosphor particles.

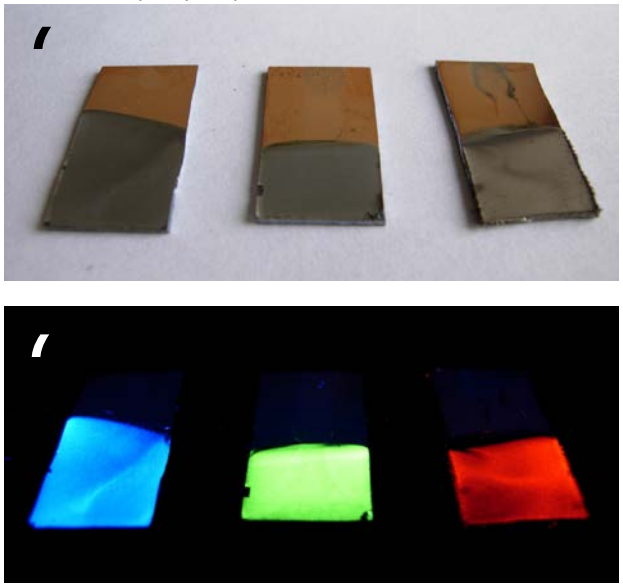

Figure 6. Samples of nickel coatings with blue emitting ($BaMg_2Al_{16}O_{27}$:Eu^{2+}), green emitting (Gd_2O_2S:Tb^{3+}) and red emitting (Y_2O_3:Eu^{3+}) rare-earth phosphor particles, (a) under daylight and (b) irradiated with short-wavelength UV light at 254 nm.

In Figure 7, the excitation and emission spectra of the initial Eu_2O_3 and Y_2O_3:Eu^{3+} particles, as well as of the Ni-Eu_2O_3 and Ni- Y_2O_3:Eu^{3+} coatings are shown. In the excitation spectra of Eu_2O_3 and Y_2O_3:Eu^{3+}, along with the broad O → Eu charge transfer band at 250-300 nm the sharp intraconfigurational f-f transitions of Eu^{3+} from the $^7F_{0,1}$ levels to $^3P_0$ (305 nm), ^5H_J (317-325 nm), $^5L_{9,10}$ (349-356 nm), $^5D_4$ (362 nm), $^5L_8$ (366 nm), ^5G_J (374-379 nm), $^5L_7$ (381 nm), $^5L_6$ (395 nm), $^5D_3$ (410 nm), $^5D_2$ (466 nm), $^5D_1$ (526 nm) are well pronounced, while for the Ni-Eu_2O_3 and Ni-Y_2O_3:Eu^{3+} coatings the charge transfer band is dominating. In addition, some expansion of the low-energy edge of the broad charge transfer band can be mentioned when going from Ni–Eu_2O_3 to Eu_2O_3 and from Ni–Y_2O_3:Eu^{3+} to Y_2O_3:Eu^{3+}. Such differences might be a result of saturation effects and/or intermolecular interactions for powder samples in comparison with the corresponding nickel coatings.[17] This effect is similar to the one observed upon dilution. In contrast, all emission spectra are very similar and show sharp lines due to mainly $^5D_0$→ ^7F_J (J = 0–4) transitions. The

similarities in crystal-field fine structure in the photoluminescence spectra indicate that the Eu^{3+} ions are at a site of the same symmetry for all samples. It is worth to note that for Eu_2O_3 and Y_2O_3:Eu^{3+} characteristic red emission of the trivalent europium ion can be also observed upon direct excitation into the $^5L_6$ level of Eu^{3+} at 395 nm, whereas for the same phosphor particles embedded in the Ni coatings no luminescence was observed upon direct excitation in the 4f levels of Eu^{3+}. The luminescence lifetime of the $^5D_0$ level in the Ni-Eu_2O_3 thin film is very short (< 0.015 ms) and much shorter than the values extracted from the bi-exponential decay of bulk Eu_2O_3, with a short component of 0.090(2) ms (85 %) and a longer one of 0.27(3) ms (15 %). This indicates that the non-radiative deactivation pathways are more efficient in the Ni coatings than in bulk Eu_2O_3. This is, however, not true for Y_2O_3:Eu^{3+} and Ni-Y_2O_3:Eu^{3+} which exhibit the same lifetimes of 1.04(1) ms. The observed lifetime lie in the range of values found in the literature for Y_2O_3:Eu^{3+} phosphors, i.e. between 0.8 and 2.0 ms.[18]

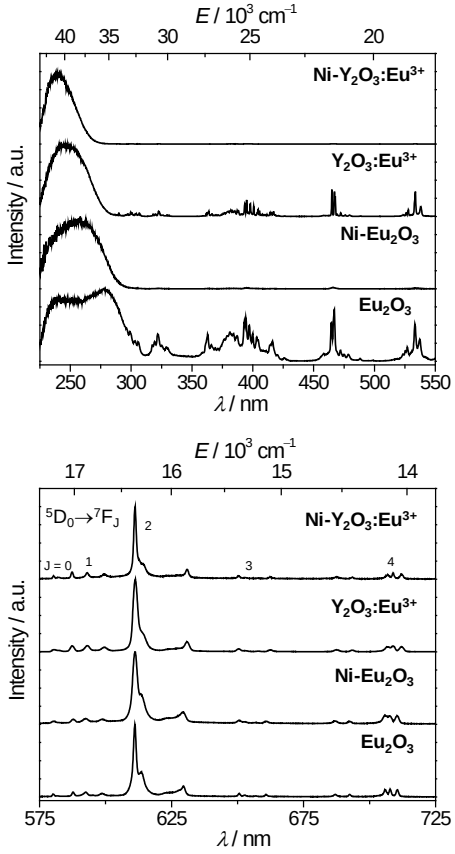

Figure 7. Room temperature excitation spectra (top; λ_{em} = 611 nm) and emission spectra (bottom; λ_{ex} = 254 nm) of Eu_2O_3 and Y_2O_3:Eu^{3+} powder and of composite nickel coatings with embedded Eu_2O_3 and Y_2O_3:Eu^{3+} particles.

The excitation spectra of the green-emitting phosphor Gd_2O_2S:Tb^{3+} and nickel coatings exhibit a broad band at circa 260 nm with a shoulder at about 290 nm due to the host lattice absorption (E_g = 4.6 eV, 270 nm) (Figure 8).[i] Sharp bands at 308 and 313 nm can be attributed to the $^6P_J \leftarrow {}^8S_{7/2}$ transitions of Gd^{3+}. The similar trend as in the case of Eu^{3+}-containing samples can be observed here for the Gd_2O_2S:Tb^{3+} powder in comparison with the Ni-Gd_2O_2S:Tb^{3+} coating, namely an increase of the intensity of f-f transitions as well as a broadening of the host-centred band, which might again be attributed to saturation effects.**Fout! Bladwijzer niet gedefinieerd.** Under excitation at 254 nm, both Gd_2O_2S:Tb^{3+} powder and nickel coating exclusively show the characteristic, narrow luminescence bands due mainly to the $^5D_4 \rightarrow {}^7F_J$ (J = 6–0) transitions (Figure 8). The integrated intensity of the $^5D_4 \rightarrow {}^7F_6$ transition increases, while these of the $^5D_4 \rightarrow {}^7F_J$ (J = 4–0) transitions decrease for the composite nickel coatings in comparison with the pure

$Gd_2O_2S:Tb^{3+}$ phosphor, when the intensities are compared relatively to that of the $^5D_4 \rightarrow {}^7F_5$ transition (Table 2). In addition, the intensity of the Tb^{3+} $^5D_3 \rightarrow {}^7F_J$ (J = 5, 4) transitions in the blue spectral range (400–450 nm) is lower for the $Gd_2O_2S:Tb^{3+}$ powder than for the corresponding nickel coating (Figure 8). Such behaviour can be explained by an increased probability of cross-relaxation, $^5D_3 + {}^7F_6 \rightarrow {}^5D_4 + {}^7F_0$, when going from Ni-$Gd_2O_2S:Tb^{3+}$, where the concentration of Tb^{3+} is lower, to the $Gd_2O_2S:Tb^{3+}$ bulk powder.[19] This effect was clearly demonstrated in case of $Y_2O_2S:Tb^{3+}$ in which the emission colour was tuned from blue to green due to the change of the dominating emitting level ($^5D_3$ to $^5D_4$) upon increasing the concentration of terbium.[20] However, the crystal-field splitting of the f-f bands and the luminescence lifetime of the $^5D_4$ level, 0.55(1) ms, remain the same after incorporation of the phosphor powder in the nickel coating. This shows that the first coordination sphere of the lanthanide ions is unaffected.

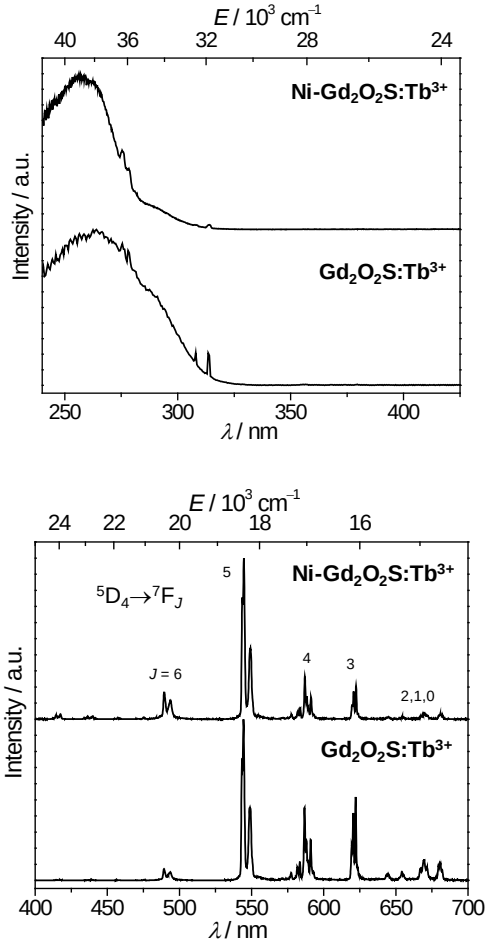

Figure 8. Room temperature excitation spectra (top; λ_{em} = 545 nm) and emission spectra (bottom; λ_{ex} = 254 nm) of $Gd_2O_2S:Tb^{3+}$ powder and of composite nickel coatings with embedded $Gd_2O_2S:Tb^{3+}$ particles.

Table 2. Relative integrated intensities of $^5D_4 \rightarrow {}^7F_J$ (*J* = 6–0) transitions in the luminescence spectrum of $Gd_2O_2S:Tb^{3+}$ and of a nickel coating with embedded $Gd_2O_2S:Tb^{3+}$ particles.

Sample	$\int_{4\text{-}6}$	$\int_{4\text{-}5}$	$\int_{4\text{-}4}$	$\int_{4\text{-}3}$	$\int_{4\text{-}2,1,0}$
$Gd_2O_2S:Tb^{3+}$	0.11	1.00[(a)]	0.50	0.37	0.38
Ni with $Gd_2O_2S:Tb^{3+}$	0.25	1.00[(a)]	0.30	0.17	0.12

[(a)] The integrated intensity of the $^5D_4 \rightarrow {}^7F_5$ transition is set to 1.00.

The blue-emitting phosphor, $BaMg_2Al_{16}O_{27}:Eu^{2+}$ (BAM: Eu^{2+}),[21] under excitation at 330 nm exhibits broad-band luminescence due to allowed 5d → 4f transitions in the range 370–570 nm centred at 455 nm. The luminescence spectra of composite nickel coatings were similar to that of the pure phosphor powder (Figure 9).

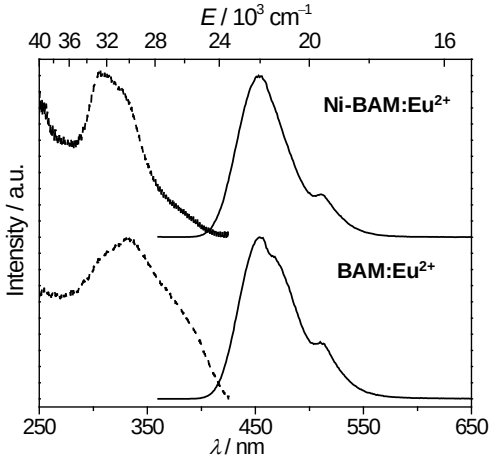

Figure 9. Room temperature excitation (dashed line; λ_{em} = 450 nm) and emission (full line; λ_{ex} = 330 nm) spectra of $BaMg_2Al_{16}O_{27}:Eu^{2+}$ powder and of composite nickel coatings with embedded $BaMg_2Al_{16}O_{27}:Eu^{2+}$ particles.

$Y_3Al_5O_{12}:Ce^{3+}$ (YAG:Ce^{3+}) powder and the corresponding composite nickel film exhibit a similar broad-band yellow-green emission centred at 550-560 nm upon excitation with a wavelength of 440 nm (Figure 10). The general envelope of the emission and excitation spectra is typical for this phosphor. Ce^{3+} exhibits broad band emission from the lowest crystal field level of the $5d^1$ excited state to the $4f^1$ ground state.[22] Upon excitation at 340 and 254 nm, the $Y_3Al_5O_{12}:Ce^{3+}$ powder and nickel film displays similar broad-band emission, but with much lower intensity than upon excitation at 440 nm (Figure S14, ESI).

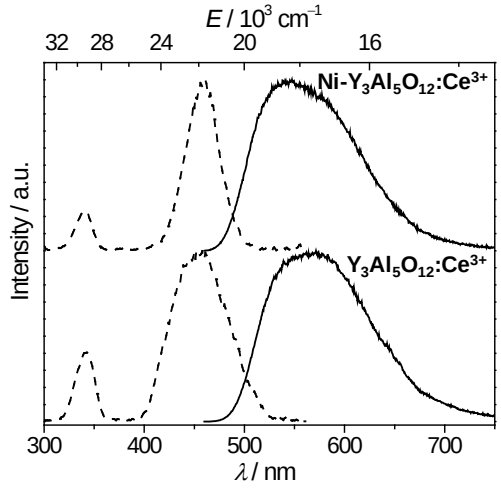

Figure 10. Room temperature excitation (dashed line; λ_{em} = 580 nm) and emission (full line; λ_{ex} = 440 nm) spectra of $Y_3Al_5O_{12}:Ce^{3+}$ powder and the corresponding composite nickel film.

In order to demonstrate the possibility of electrodeposition of colour-tuneable composite Ni coatings, the mixtures of red ($Y_2O_3:Eu^{3+}$) and green ($Gd_2O_2S:Tb^{3+}$) phosphors in 90:10, 75:25, 50:50, 25:75 and 10:90 Eu/Tb wt. % ratios were prepared. The corresponding luminescence spectra are shown in Figure S15, ESI. The spectra present a superposition of the corresponding $Y_2O_3:Eu^{3+}$ and $Gd_2O_2S:Tb^{3+}$ phosphors and an

almost linear dependence of the luminescence intensity of the $^5D_0 \rightarrow {}^7F_2$ (Eu) or the $^5D_4 \rightarrow {}^7F_5$ (Tb) on the phosphor concentration was observed (Figure 11). Such behaviour is typical for systems where there is no energy transfer from Tb^{3+} to Eu^{3+}. This was further confirmed by luminescence lifetime measurements: τ_{obs} of the both Eu($^5D_0$) and Tb($^5D_4$) levels remain the same within experimental errors, 1.02(1) and 0.57(2) ms, to that of the initial phosphors (Table S3, ESI). Calculation of the CIE colour coordinates for the pure phosphors and their 75:25, 50:50, 25:75 and 10:90 Eu/Tb wt. % mixtures demonstrates that the emission colour can be continuously tuned from red (0.652; 0.345) to green (0.411; 0.537) (Figure 12 and Table S4, ESI). Composite Ni coatings were prepared using the mixtures with 50:50 and 25:75 Eu/Tb wt.% ratios under the same experimental condition as for the pure phosphors. SEM images and EDX spectra of these coating demonstrate that the ratio of the phosphors in the coatings remains the same as in the original phosphor mixtures (Figure S18, ESI). This indicates that with nickel there is no preferential incorporation of one type of phosphor over another.

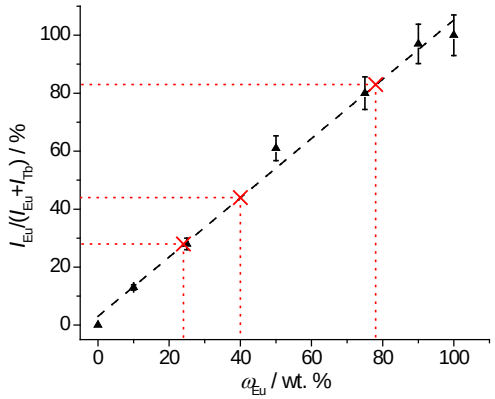

Figure 11. Intensity of the $^5D_0 \rightarrow {}^7F_2$ transition (I_{Eu}) relative to the sum of I_{Eu} and I_{Tb} ($^5D_4 \rightarrow {}^7F_5$ transition), derived from the luminescence spectra of the powder samples of the red and green phosphors and mixtures of them, versus the Y_2O_3:Eu^{3+} content. The dashed line represents the linear fit and the red crosses reflect the composition of the corresponding nickel coatings.

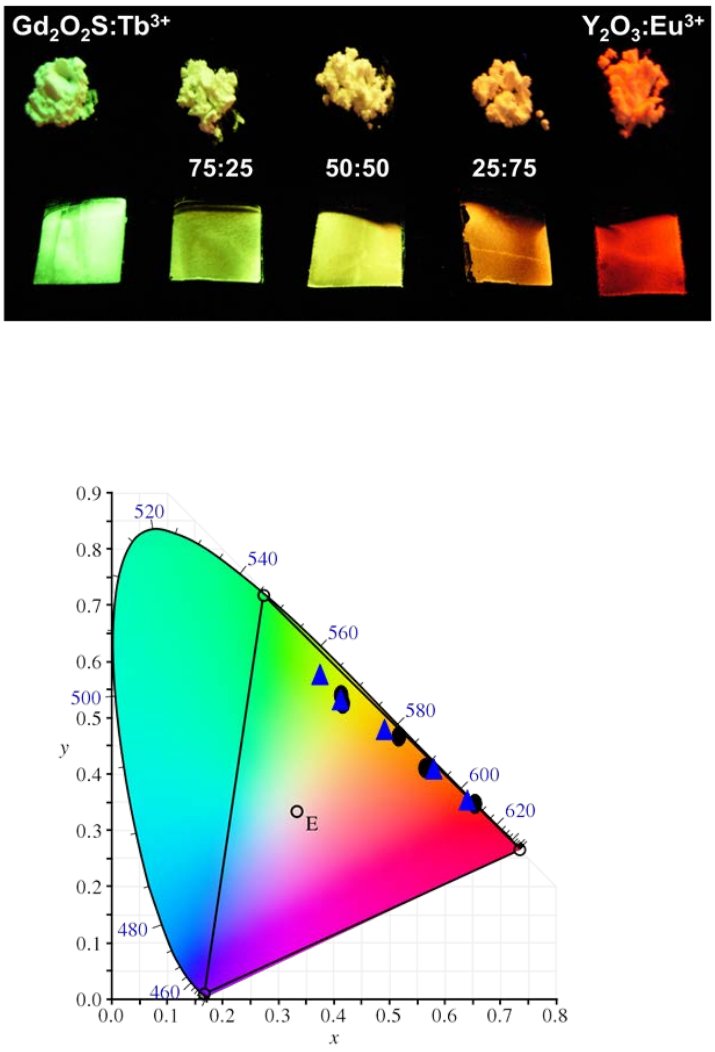

Figure 12. (Top) Photos of green-emitting $Gd_2O_2S:Tb^{3+}$ powder and red-emitting $Y_2O_3:Eu^{3+}$ powder and different mixtures of them, as well as the corresponding composite nickel coatings under 254 nm excitation and (bottom) CIE trichromatic coordinates (black circles: powders; blue triangles: nickel coatings).

The luminescence spectra of the obtained composite nickel coatings are presented on Figure 13 and exhibit both the $^5D_0 \rightarrow {}^7F_J$ and the $^5D_4 \rightarrow {}^7F_J$ transitions. Their photos under UV irradiation are shown in Figure 12(top). The luminescence lifetimes were measured for all nickel coatings and proved to be unchanged (Table S3, ESI). If one considers the relative intensity of the $^5D_0 \rightarrow {}^7F_2$ transition and the linear fit in Figure 11, the content of the red phosphor in the composite Ni coatings can be calculated: 24, 40 and 78 wt.%, instead of, respectively, 25, 50 and 75 wt.% for the initially used mixtures. The calculated colour coordinates (Figure 12(bottom) and Table S4, ESI) are in agreement with the dependence of the relative intensity of the $^5D_0 \rightarrow {}^7F_2$ transition. A good correlation was observed for the nickel coatings prepared from 25:75 and 75:25 Eu/Tb wt.% mixtures, while the highest deviation was detected for that from the 50:50 Eu/Tb wt.% mixture. It is worth noting that CIE coordinates of the $Y_2O_3:Eu^{3+}$ powder (0.652; 0.345) and the corresponding nickel coating (0.638; 0.346) match very well, while a significant variation can be mentioned for the Tb^{3+}-containing samples. This, however, can be explained by the discussed above difference in relative integral intensities of $^5D_4 \rightarrow {}^7F_J$ transitions (Table 2) and an increased probability of emission from the $^5D_3$ level in case of the Ni- $Gd_2O_2S:Tb^{3+}$ coating.

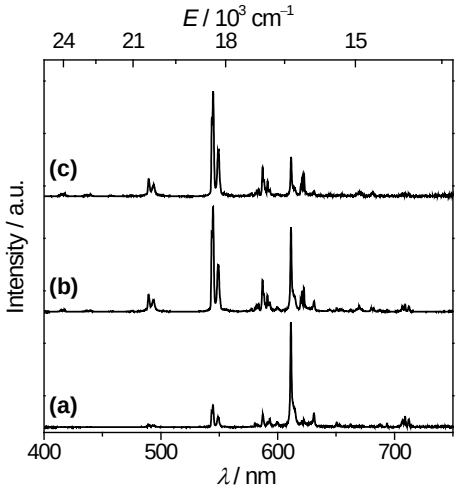

Figure 13. Room temperature emission spectra (λ_{ex} = 254 nm) of the mixtures of red $Y_2O_3:Eu^{3+}$ and green $Gd_2O_2S:Tb^{3+}$ phosphors in the following weight ratios: (a) 75:25, (b) 50:50 and (c) 25:75, respectively.

A possibility of obtaining white-emitting phosphors and metal coatings by an appropriate mixing was also tested. As a first try, a 50:50 wt.% mixture of yellow (YAG: Ce^{3+}) and blue (BAM: Eu^{2+}) phosphor powders was prepared. The luminescence spectra under UV excitation (Figure S16, ESI) in general present a superposition of the corresponding emission spectra of the pure phosphors (Figures 9, 10), however a dip can be seen at circa 470 nm which corresponds to the absorption of the YAG: Ce^{3+}. Shifting of the excitation wavelengths from 254 to 340 nm resulted in an increase of yellow emission component at about 570 nm, as a consequence, the colour coordinates change, from (0.257; 0.312) to (0.300; 0.353), and become closer to the values of ideal white light (0.33; 0.33) (Figure S17, ESI). However, the preparation of the nickel coatings with similar luminescent properties appeared to be less straightforward than in the case of the red/green mixtures. The luminescence spectra of the nickel coatings obtained using a 50:50 wt.% mixture were lacking a yellow component under both 254 and 340 nm excitation (Figure S16, ESI). The CIE coordinates reflect this change and shift to the blue region: (0.15; 0.11) (Figure S17, ESI).

Conclusions

Mixtures of acetamide and dimethylsulfone with dissolved anhydrous transition metal chlorides are excellent non-aqueous electrolytes for the preparation of composite metal coatings containing hydrophilic particles via an electrolytic co-deposition process. This is illustrated for nickel and cobalt coatings with embedded rare-earth phosphor particles. Luminescence studies have demonstrated that phosphor particles remain unaffected when incorporated into the nickel coatings. Furthermore, the nickel coatings with colours ranging from red to green can be obtained by simply using mixtures of the corresponding phosphors for the electrodeposition. These materials have properties that are quite different from those of thin films of hybrid materials where phosphor particles are dispersed into a polymer or sol-gel matrix. The coatings have a metallic lustre and they are photoluminescent upon irradiation with UV light. The composite metal coatings are of course not transparent, so that the emission is originating only from the phosphor particles that are exposed on the surface of the coating and not from the particles in the bulk of the metal coating. However, the metal coatings have superior mechanical properties and thermal stability compared to the conventional hybrid materials. They are not brittle and they are resistant against abrasion. Moreover, the composite metal coatings are good conductors of electricity.

Acknowledgements

The authors acknowledge financial support by the K.U.Leuven (project and GOA 08/05), by the FWO-Flanders (research community “Ionic Liquids” and project G.0508.07) and by the IWT-Flanders (SBO-project “MAPIL”) and the Belgian Federal Science Policy Office through the IUAP project INANOMAT (contract P6/17). MG thanks the K.U.Leuven for a PhD fellowship (DBOF grant). SVE is a visiting postdoctoral fellow of FWO-Flanders (project G.0412.09).

Electronic supplementary information

Electronic supplementary information (ESI) available: Additional SEM pictures and EDX spectra; tables with results of variation of the deposition parameters; picture of the nickel coatings with $Y_3Al_5O_{12}:Ce^{3+}$ under daylight and UV illumination; luminescence spectra of $Y_3Al_5O_{12}:Ce^{3+}$ excited at different wavelengths; excitation spectra of Eu_2O_3 and $Gd_2O_2S:Tb^{3+}$ depending on the thickness of the phosphor layer; luminescence spectra, lifetimes and CIE coordinates of the mixtures of phosphors.

REFERENCES

1 (a) J. R. Roos, J. P. Celis, J. Fransaer and C. Buelens, *JOM-J. Min. Met. Mat Soc.,* 1990, **42**, 60; (b) A. Hovestad and L. J. J. Janssen, *J. Appl. Electrochem.*, 1995, **25**, 519; (c) C. T. J. Low, R. G. A. Wills and F. C. Walsh, *Surf. Coat. Technol.*, 2006, **201**, 371; (d) J. N. Balaraju, T. S. N. S. Narayanan and S. K. Seshadri, *J. Appl. Electrochem.*, 2003, **33**, 807; (e) V. P. Greco, V. P. *Plat. Surf. Finish.*, 1989, **76**, 62; (f) J. P. Celis, J. R. Roos, C. Buelens and J. Fransaer, *Trans. Inst. Met. Fin.*,1991, **69**, 133; (g) N. Feldstein, T. Lancsek, D. Lindsay and L. Salerno, *Met. Finish.,* 1983, **81**, 35; (h) A. P. Abbott, K. El Ttaib, G. Frisch, K. J. McKenzie and K. S. Ryder, *Phys. Chem. Chem. Phys.*, 2009, **11**, 4269.

2 (a) A. F. Zimmerman, D. G. Clark, K. T. Aust and U. Erb, *Mater. Lett.*, 2002, **52**, 85; (b) K. H. Hou, M. D. Ger, L. M. Wang and S. T. Ke, *Wear*, 2002, **253**, 994; (c) M. Lekka, N. Kouloumbi, M. Gajo and P. L. Bonora, *Electrochim. Acta*, 2005, **50**, 4551; (d) I. Garcia, J. Fransaer and J. P. Celis, *Surf. Coat. Technol.*, 2001, **148**, 171; (e) M. D. Feldstein, *Plat. Surf. Finish.,* 1998*, 85,* 248; (f) H. AbiAkar, C. Riley and G. Maybee, *Chem. Mater.*, 1996, **8**, 2601.

3 (a) P. R. Ebdon, *Plat. Surf. Finish.*, 1988, **75**, 65; (b) M. Pushpavanam, N. Arivalagan, N. Srinivasan, P. Santhakumar and S. Suresh, *Plat. Surf. Finish.*, 1996, **81**, 72.

4 M. D. Feldstein, *Metal. Finish.*, 1999, **97**, 87.

5 N. Feldstein, *US Patent Application* 5,516,591 (1996).

6 C. M. Das, A. K. Grover and A. K. Suri, *Trans. Inst. Met. Finish.*, 2002, **80**, 128.

7 (a) M. Bredol, U. Kynast, C. Ronda, *Adv. Mater.*, 1991, **3**, 361; (b) T. Jüstel, H. Nikol and C. Ronda, *Angew. Chem. Int. Ed. Engl.*, 1998, **37**, 3085; (c) S. V. Eliseeva and J.-C. G Bünzli, *Chem. Soc. Rev.*, 2010, **39**, 189; (d) J.-C. G. Bünzli and C. Piguet, *Chem. Soc. Rev.*, 2005, **34**, 1048; (e) K. Binnemans, *Chem. Rev.,* 2009, **109**, 4283; f) L. D. Carlos, R. A. S. Ferreira, V. De Zea Bermudez and S. J. L. Ribeiro, *Adv. Mater.*, 2009, **21**, 509.

8 http://www.surfacetechnology.com/lec.html (accessed on 21 December 2011).

9 (a) Z. Y. Zhang, X. C. Lu, A. L. Han and H. B. Luo, *Mater. Sci. Eng. A*, 2007, **454**, 194; (b) S. P. Sharma, D. K. Dwivedi and P. K. Jain, *Wear*, 2009, **267**, 853. (c) X. Z. Liu, X. Li, A. B. Yu, A.B. and W. J. Huang, *J. Rare Earths*, 2009, **27**, 480. (d) R. D. Xu, J. L. Wang, Z. C. Guo, and H. Wang, *J. Rare Earths*, 2008, **26**, 579.

10 (a) L. Stappers and J. Fransaer, *J. Electrochem. Soc.*, 2006, **153**, C472; (b) L. Stappers and J. Fransaer, *J. Electrochem. Soc.*, 2007, **154**, D598.

11 (a) J. Fransaer, E. Leunis, T. Hirato and J. P.Celis, *J. Appl. Electrochem.*, 2002, **32**, 123; (b) T. Hirato, J. Fransaer and J. P. Celis, *J. Electrochem. Soc.*, *2001*, **148**, C280.

12 (a) Y. G. Zhao and T. J. VanderNoot, *Electrochim. Acta*, 1997, **42**, 3; (b) L. Legrand, M. Heintz, A. Tranchant and R. Messina, *Electrochim. Acta*, 1995, **40**, 1711; (c) T. Jiang, M. J. C. Brym, G. Dube, A. Lasia and G. M. Brisard, *Surf. Coat. Technol.*, 2007, **201**, 6309; (d) C. C. Yang and M. F. Shu, *Z. Naturforsch. A*, 2007, **62**, 754.

13 (a) P. Liu, Y. P. Du, Q. Q. Yang, G. R. Li and Y. X. Tong, *Electrochim. Acta*, 2006, *52*, 710; (b) P. Liu, Q. Q. Yang, Y. S. Yang and Y.X. Tong, *J. Rare Earths*, 1999, **17**, 151.

14 G. Tammann, *Z. Anorg. Chem.*, 1903, **37**, 303.

15 (a) F. J. Martinez Casado, M. Ramos Riesco, I. Da Silva, A. Labrador, M. I. Redondo, M. V. Garcia-Perez, M. V.; S. Lopez-Andres and J. A. R. Cheda, *J. Phys. Chem. B*, 2010, **114**, 10075; (b) F. J. Martınez Casado, M. Ramos Riesco, M. and J. A. R. Cheda, *J. Therm. Anal. Calorim.*, 2007, **87**, 73.

16 (a) G. Blasse and Grabmaier, *Luminescent Materials*, Springer-Verlag, Berlin, 1994; (b) G. Blasse, *J. Alloys Compds.*, 1993, **192**, 17.

17 C. D. M. Donega, A. Meijerink and G. Blasse, *J. Lumin.*, 1994, **62**, 189.

18 (a) H. Wang, C. K. Lin, X. M. Liu, J. Lin and M. Yu, *Appl. Phys. Lett.*, 2005, **87**, 181907; (b) M. L. Pang, J. Lin, Z. Y. Cheng, J. Fu, R. B. Xing and S. B. Wang, *Mater. Sci. Eng. B*, 2003, **100**, 124; (c) G. Jia, M. Yang, Y. H.; Song, H.P. You and H. J. Zhang, *Cryst. Growth Des.*, 2009, **9**, 301; (d) D. K. Williams, B. Bihari, B. M. Tissue and J. M. McHale, *J. Phys. Chem. B*, 1998, **102**, 916.

19 (a) Y. Tian, W. H. Cao, X. X. Luo and Y. Fu, *J. Alloys Compds.*, 2007, **433**, 313; (b) M. D. Faucher, R. Morlotti and O. K. Moune, *J. Lumin.*, 2002, **96**, 37; (c) J. Hölsä, M. Leskela and L. Niinisto, *Mater. Res. Bull.* 1979, **14**, 1403.

20 C. C. Kang and R. S. Liu, *J. Lumin.*, 2001, **122-123** , 574.

21 S. Ekambaram and K. C. Patil, *J. Alloys Compds.*, 1997, **248**, 7.

22 (a) V. Bachmann, C. Ronda and A. Meijerink, *Chem. Mater.* 2009, **21**, 2077; (b) N. P. Jia, X. D. Zhang, W. He, W. J. Hu, X.P. Meng, Y. Du, J. C. Jiang and Y. W. Du, *J. Alloys Compd.*, 2011, **509**, 1848; (c) K. Y. Jung and Y. C. Kang, *Physica B*, 2010, **405**, 1615.

Dienst Onderzoekscoördinatie
Huis Bethlehem
Schapenstraat 34
B-3000 Leuven
België
Tel.: +32 16 32 40 65
Fax: +32 16 32 41 98
onderzoek@kuleuven.be
www.kuleuven.be